# Ammonia-free fabrication of ultrafine vanadium nitride nanoparticles as interfacial mediators for promoting electrochemical behaviors of lithium-sulfur batteries

Xueping Meng,[a,c] Zhonglin Li,[b,c] Zhibin Cheng,[a] Pengyue Li,[a,b] Ruihu Wang[b,c] and Xiaoju Li*[,a,b]

[a]Fujian Provincial Key Laboratory of Polymer Materials, College of Chemistry and Materials Science, Fujian Normal University, Fuzhou, Fujian 350007, China

*E-mail: xiaojuli@fjnu.edu.cn

[b]Tianjin Key Laboratory of Chemical Process Safety, School of Chemical Engineering and Technology, Hebei University of Technology, Tianjin 300130, China

[c]State Key Laboratory of Structural Chemistry, Fujian Institute of Research on the Structure of Matter, Chinese Academy of Sciences, Fuzhou, Fujian 350002, China.

**Structure characterization**

Powder X-ray diffraction (XRD) patterns were obtained in the range of 2θ = 5 - 80° on a desktop X-ray diffractometer (RIGAKU-Miniflex 600) using Cu Kα radiation. X-ray photoelectron spectroscopy (XPS) measurements were recorded by a Thermo ESCALAB 250 spectrometer with a nonmonochromatic Al Kα X-ray as the excitation source and choosing C 1s (284.7 eV) as the reference line to analyze the surface species and their chemical states. Raman spectra were recorded on a Renishaw in Via system by using 532 nm incident radiation. Thermogravimetric analysis (TGA) was measured at a heating rate of 10 ℃ $min^{-1}$ using a STA449 C Jupiter thermo gravimetric analyzer (NETZSCH). The inductively coupled plasma atom emission spectrometry (ICP-AES) was measured on Jobin Yvon Ultima 2. Nitrogen adsorption/desorption data were recorded at the liquid nitrogen temperature (77 K) using a Micromeritics ASAP 2020 M apparatus. The samples were degassed at 120 ℃ under vacuum for 10 h prior to the measurement. The specific surface area was calculated using the Brunauer-Emmett-Teller (BET) equation, and the total pore volumes were calculated from the amount adsorbed at a relative pressure ($P/P_0$) of 0.99. The pore size distributions were calculated by the nonlocal density functional theory (NLDFT) model. Scanning electron microscope (SEM) images were obtained with a JSM-6700F field-emission scan electron microscope. Transmission electron microscope (TEM) images were obtained on TECNAI G2F20. Liquid UV-Vis spectroscopic analyses were performed on a Lambda35 UV-Vis spectrophotometer.

**Electrochemical Characterization**

Electrochemical experiments were performed via CR2025 coin-type test cells assembled with lithium metal as the counter and reference electrode in an argon-filled glove box, in which the moisture and oxygen levels were both kept below 1.0 ppm. Celgard 2400 membrane was used as the separator to isolate electrons. The electrolyte was 1 M lithium bis(trifluoromethane)sulfonamide with 1% anhydrous $LiNO_3$ dissolved in a mixture of 1,3-

dioxolane and dimethoxymethane (1:1 by volume). The discharge/charge measurements were conducted at a voltage interval of 1.7 to 2.8 V using a Neware battery test system (Neware Technology Co.). Before testing, the cells were aged for 24 h. Cyclic voltammetry (CV) and electrochemical impedance spectroscopy (EIS) measurements were performed on CHI604E electrochemical workstation. The CV scan rate was fixed at 0.1 mV $s^{-1}$ and EIS was measured with an applied sinusoidal excitation voltage of 5 mV in the frequency range from 100 kHz to 0.1 Hz.

**Adsorption test of lithium polysulfides**

All the samples were dried at 60 ºC under vacuum overnight before conducting the adsorption test. Under the $N_2$ atmosphere, the mixture of sulfur and lithium sulfide with the molar ratio of 5:1 were dispersed in tetrahydrofuran (THF) at 60 ºC maintain 12 h to prepare a brownish-red $Li_2S_6$ stock solution (0.5 M). The adsorption capabilities of active material were explored by equivalent amounts (30 mg) of carbon host was added into the diluted stock solution (3 mL, 10 mM) solution. The filtered supernatant was pipetted for visual detection and Ultraviolet-visible measurement.

**Preparation of the Electrodes**

Active materials (VN@NPC/CNT-T-65S and NPC/CNT-800-63S), acetylene black, and polyvinylidene fluoride were mixed with the weight ratio of 75:15:10 were dispersed in 1-methyl-2-pyrrolidinone (NMP) and stirred to form a homogeneous slurry. The slurry was then pasted onto an Al-foil current collector, baked at 60 °C under vacuum overnight, subsequently, the dried slurry on aluminum foil and punched into small circular electrodes and stored them in Ar-filled glovebox for the assembly of the cells.

**Symmetrical cell assembly and measurements**

The electrodes for symmetrical cells were constructed with VN@NPC/CNT-T and NPC/CNT-800 as the work and counter electrodes in the absence of sulfur. Under normal conditions, the mixture of each active material and polyvinylidene difluoride (PVDF) binder

were dispersed in NMP with a weight ratio of 4:1. The obtained slurry was coated onto Al foil using a doctor blade, which was followed by thorough drying. After that, small discs with a diameter of 14.0 mm were punched out of slurry-coated aluminum foils after dried overnight. The areal sulfur loading within the coin cells (VN@NPC/CNT-T and NPC/CNT-800) was around 2.0 mg $cm^{-2}$. The electrolyte used was $Li_2S_6$ solution (0.5 M), wherein the dosage of electrolyte was 60 uL in each electrode. CV measurements were conducted at 3 mV $s^{-1}$ within the voltage range of -1.0 V -1.0 V. All of the above processes were carried out in a glove box filled with argon (with oxygen and moisture levels were both maintain below 1.0 ppm). Electrochemical impedance spectroscopy (EIS) was measured at open circuit potential by applying sinusoidal potential with an amplitude of 10 mV in a sweeping frequency range between 200 kHz and 0.02 Hz.

**Measurement of the $Li_2S$ nucleation on different reactive surfaces**

Nucleation measurement was probed in standard 2025 coin cells, in which lithium foil serves as the counter electrode, a new electrode in the aforementioned kinetic study as the working electrode and two electrodes were separated by Celgard 2400 membrane. $Li_2S_8$ solution was prepared by mixing lithium sulfide and sulfur powders with a molar ratio of 1:7 in tetraglyme solvent, followed by stirring. 20 uL $Li_2S_8$ solution was used as catholyte, while 20 uL blank electrolyte that was otherwise identical but without $Li_2S_8$ was applied as anolyte. The assembled cells were first discharge galvanostatically at the current of 0.112 mA until the potential reach to 2.06 V, then maintain discharged potentiostatically at 2.05 V for $Li_2S$ to nucleate and grow and discharge process was terminated when the current was decreased to $10^{-5}$ A. The discharge data was collected for analysis of the nucleation and growth rate of $Li_2S$ based on Faraday's law. The disassembled cells after discharge were used to study $Li_2S$ deposition morphology on different substances.

**The calculation for average decay rate of the electrode**

The average capacity decay rate per cycle $v$ is obtained from formula (1), where $C_{in}$, $C_{re}$ and

$N_{cyc}$ represent the initial capacity, the retention capacity after cycling and the cycling numbers, respectively.

$$v = [(C_{in} - C_{re})/ C_{in}]/ N_{cyc} *100 \text{ wt\%} \quad (1)$$

For example, when the electrode delivers the initial capacity of 963 mA h $g^{-1}$ at 1 C, and the capacity is maintained at 624 mA h $g^{-1}$ after 1000 cycles, the following average decay rate can be obtained.

v = [(963 mA h $g^{-1}$ - 624 mA h $g^{-1}$)/ 963 mA h $g^{-1}$]/ 1000 *100 wt% ≈ 0.03 wt%."

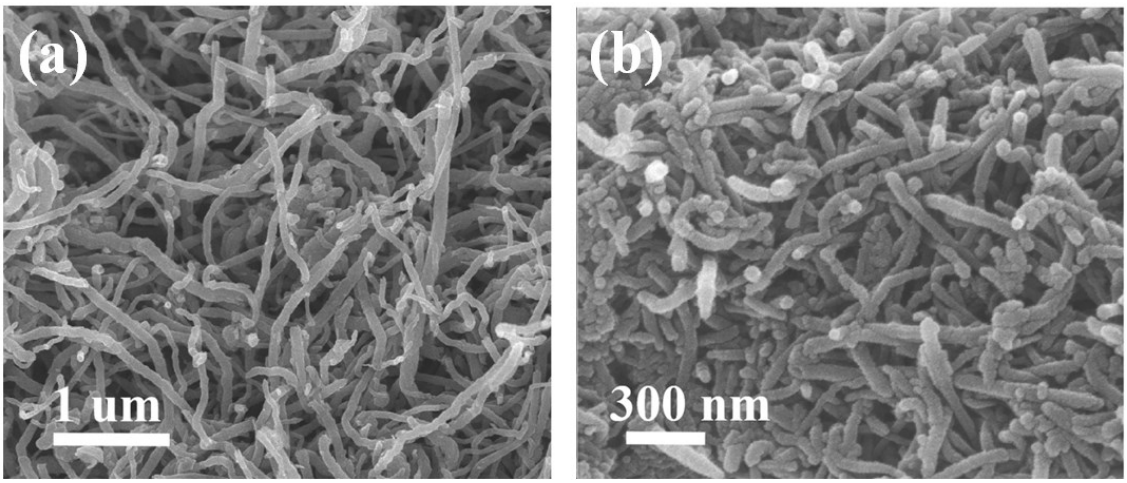


**Fig. S1** SEM images of CNTs.

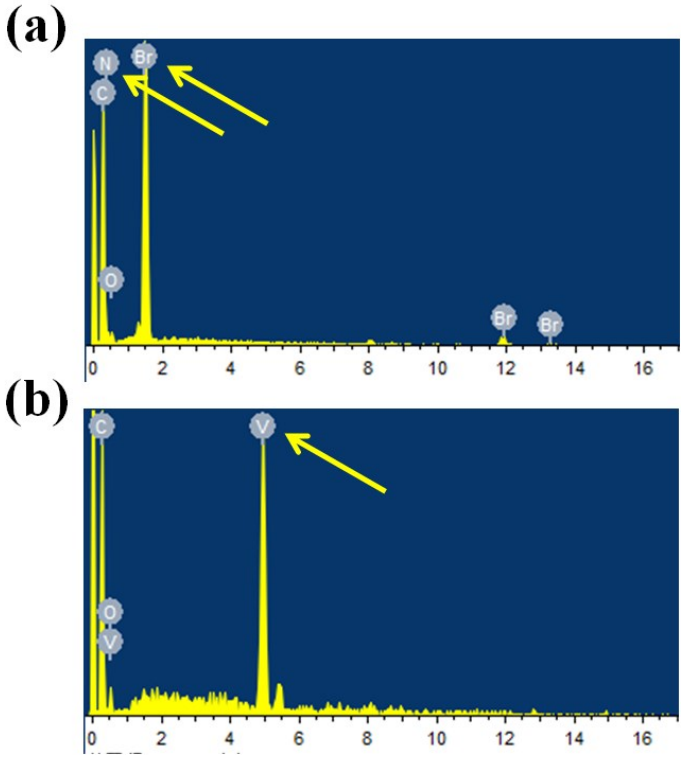


**Fig. S2** EDX elementary analysis of (a) CNT/ImIP-Br and (b) CNT/ImIP-V.

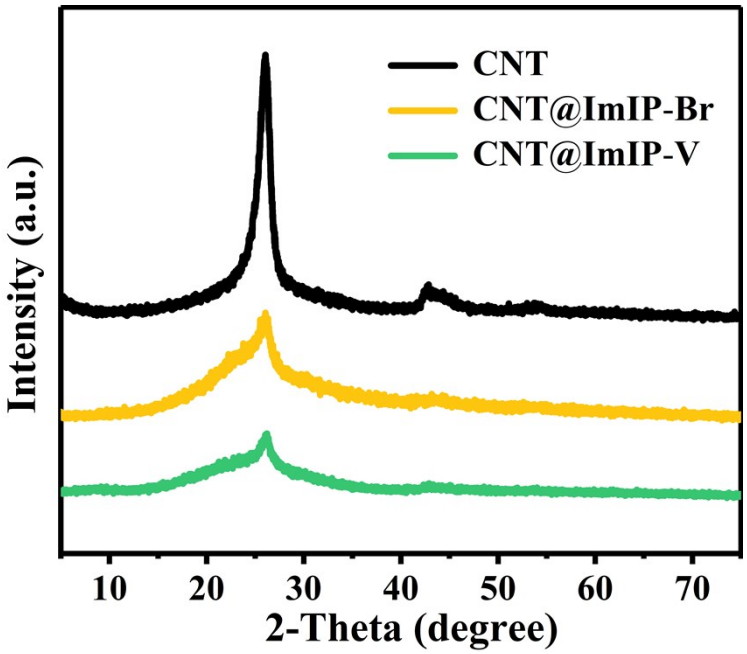


**Fig. S3** XRD patterns of CNTs, CNT/ImIP-Br and CNT/ImIP-V.

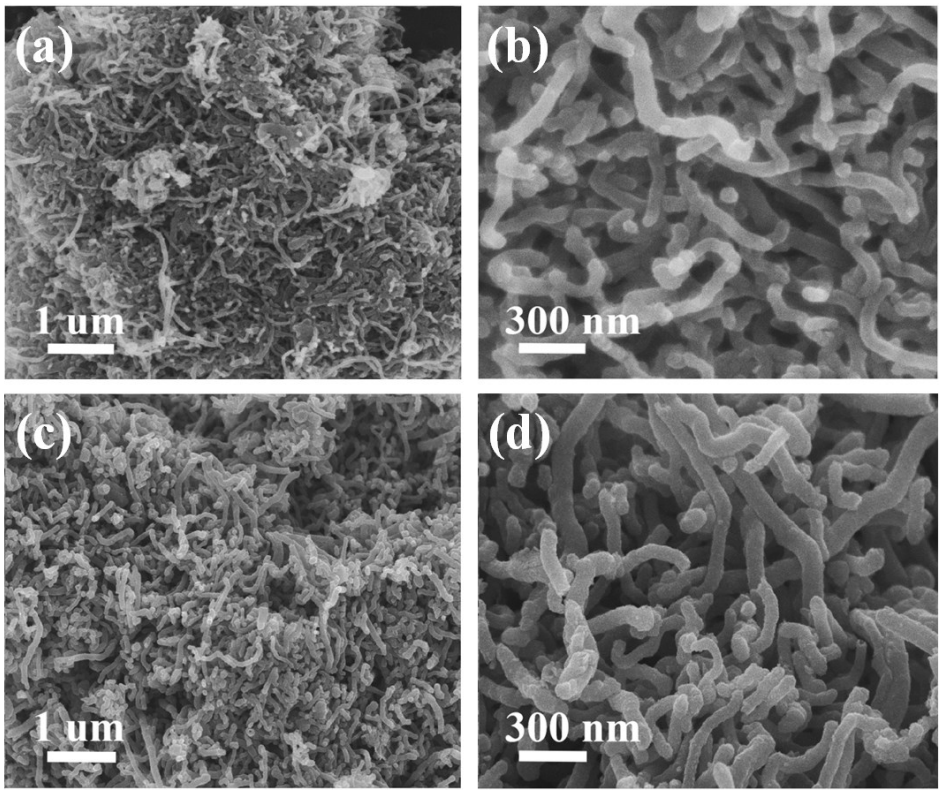


**Fig. S4** SEM images for (a,b) VN@NPC/CNT-700 and (c,d) VN@NPC/CNT-900.

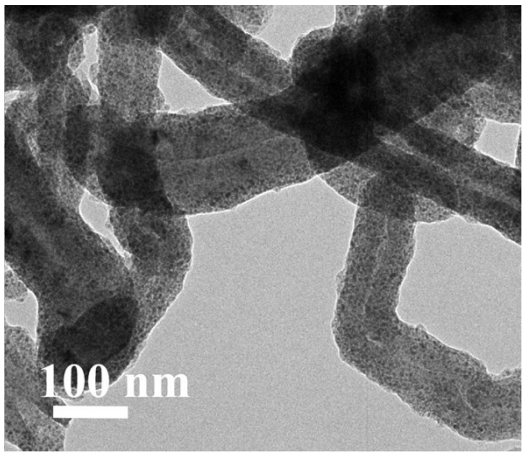


**Fig. S5** (a, b) TEM images for VN@NPC/CNT-800.

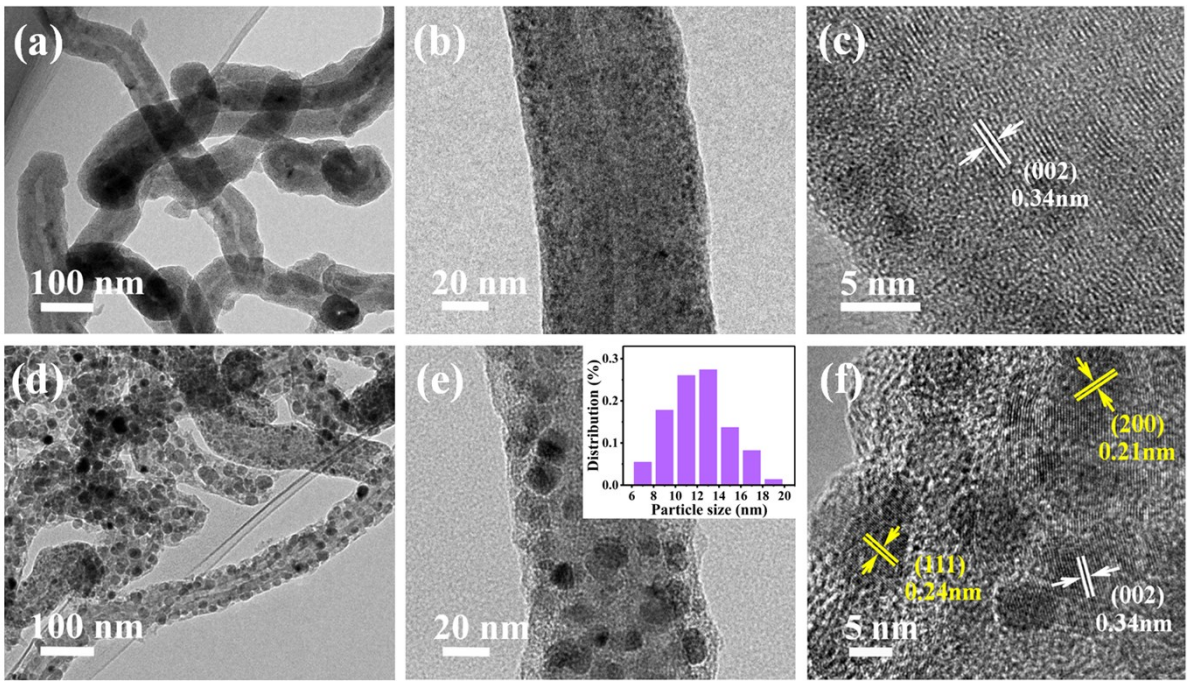


**Fig. S6** (a, b) TEM and (c) HRTEM images for VN@NPC/CNT-700. (d, e) TEM and (f) HRTEM images for VN@NPC/CNT-900. The inset in e is particle size distribution.

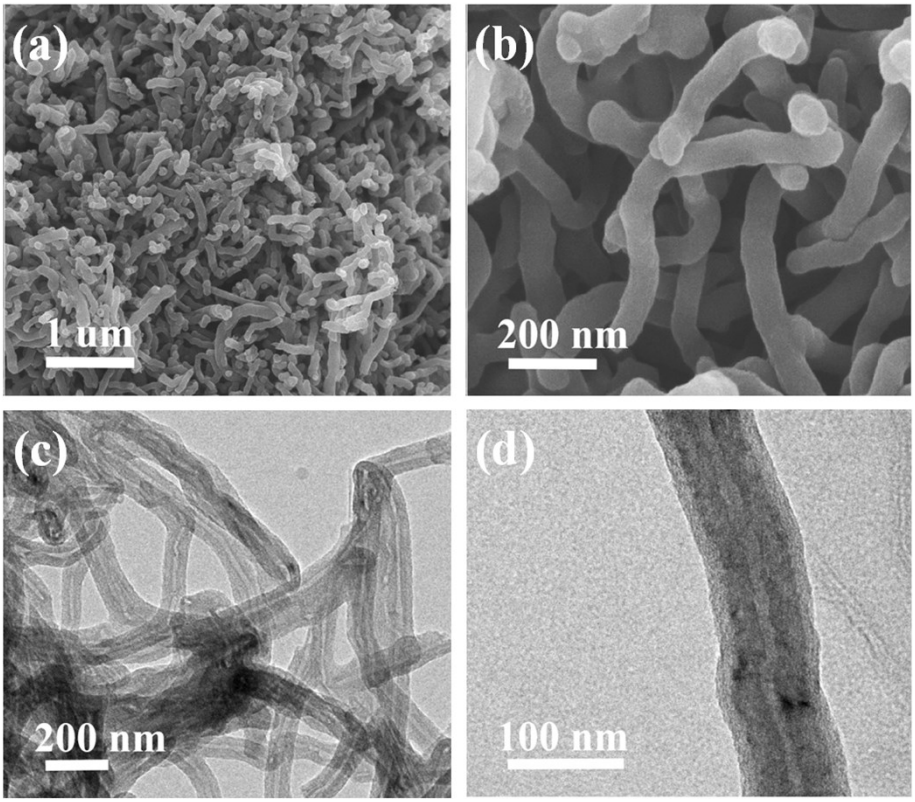


**Fig. S7** (a,b) SEM and (c,d)TEM images for NPC/CNT-800.

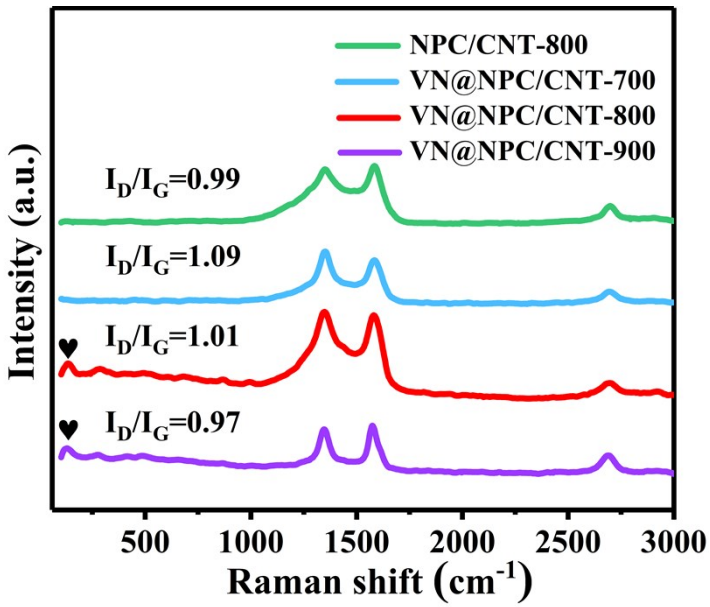


**Fig. S8** Raman spectra of NPC/CNT-800 and VN@NPC/CNT-T.

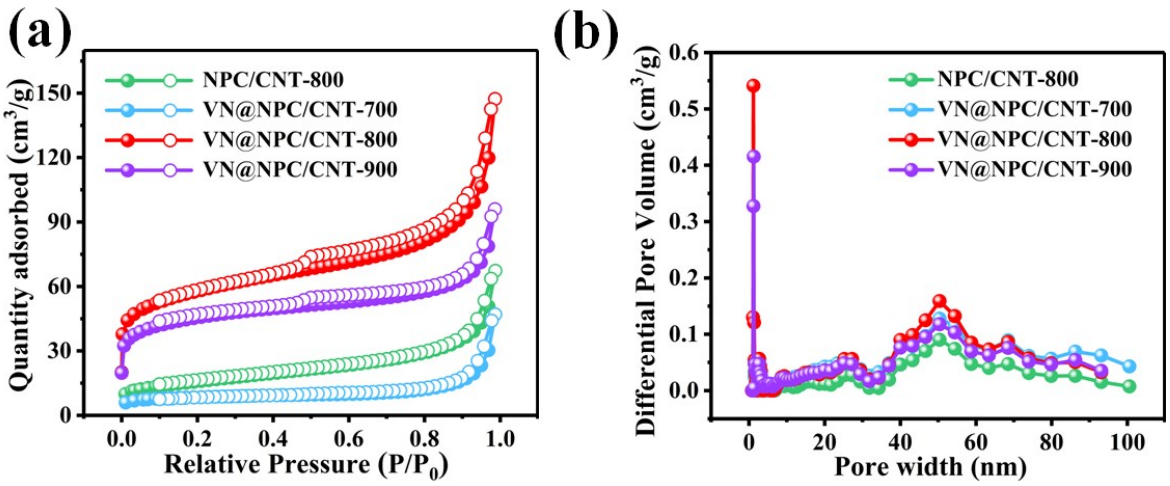


**Fig. S9** (a) $N_2$ adsorption-desorption isotherms and (b) pore size distribution plots of VN@NPC/CNT-T and NPC/CNT-800.

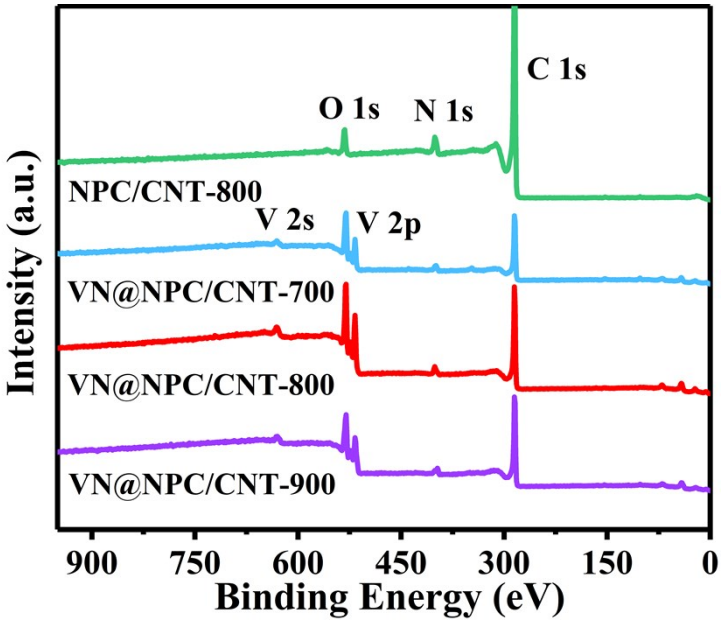


**Fig. S10** XPS survey spectra for VN@NPC/CNT-T and NPC/CNT-800.

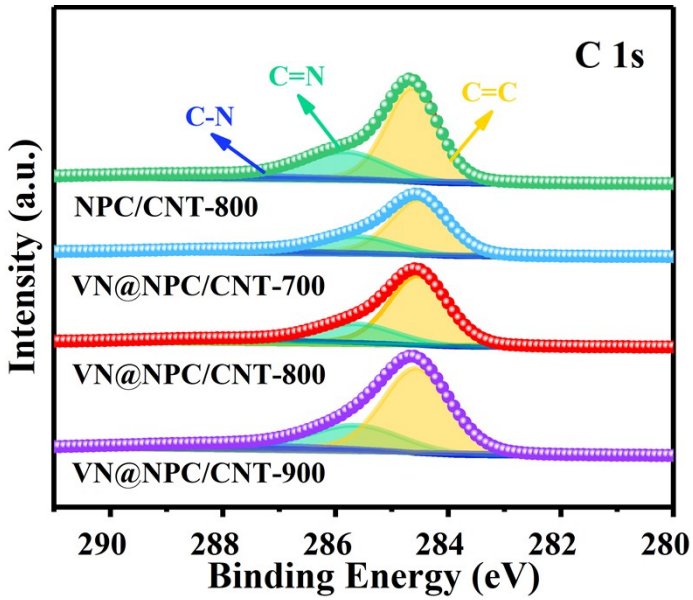


**Fig. S11** High resolution C 1s XPS spectra of VN@NPC/CNT-T and NPC/CNT-800.

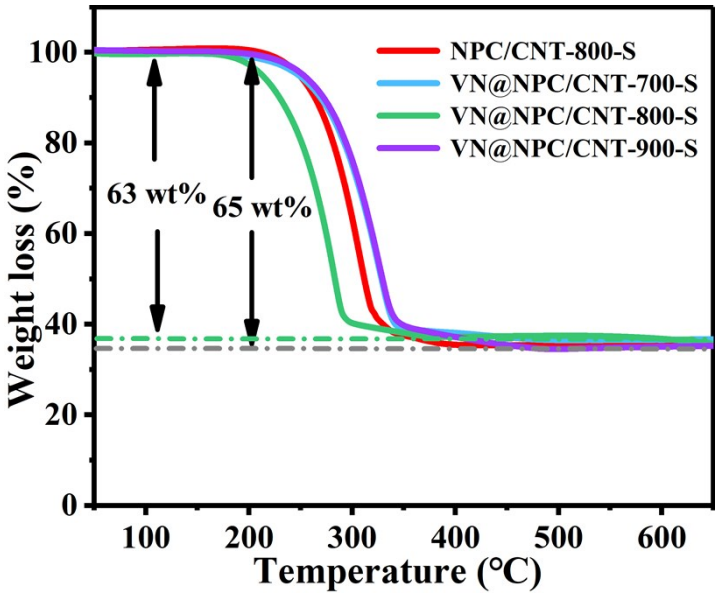


**Fig. S12** TGA curves for VN@NPC/CNT-T-S and NPC/CNT-800-S.

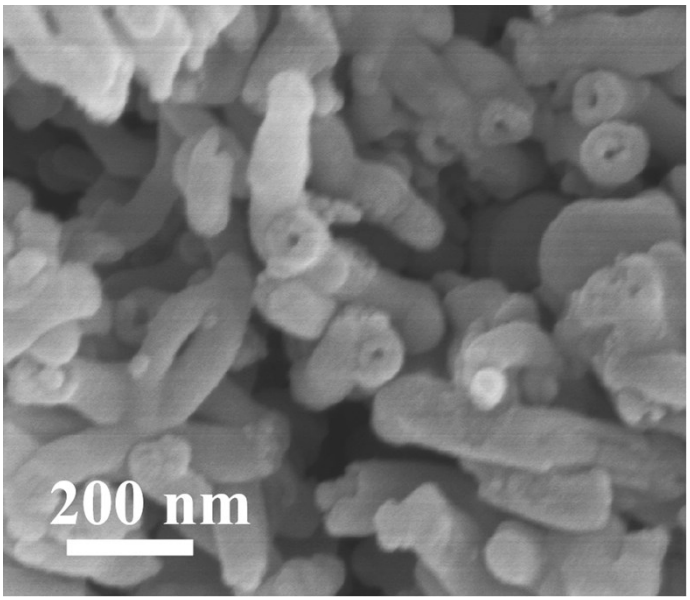


**Fig. S13** SEM image of VN@NPC/CNT-800-S.

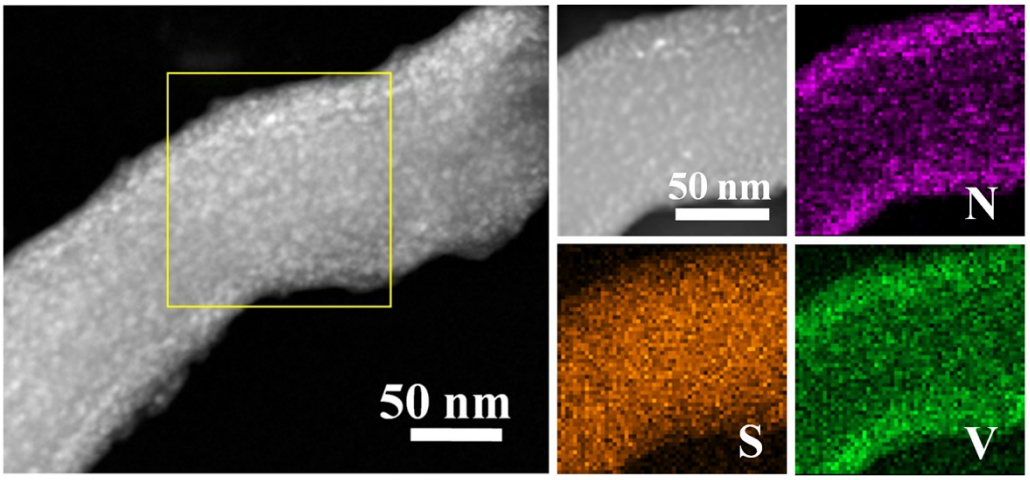


**Fig. S14** TEM images and and the cooresponding elemental mappings of VN@NPC/CNT-800-S.

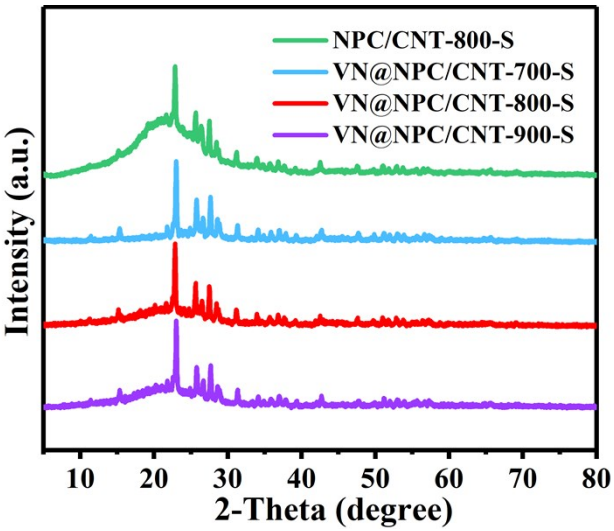


**Fig. S15** XRD patterns of VN@NPC/CNT-T-S and NPC/CNT-800-S.

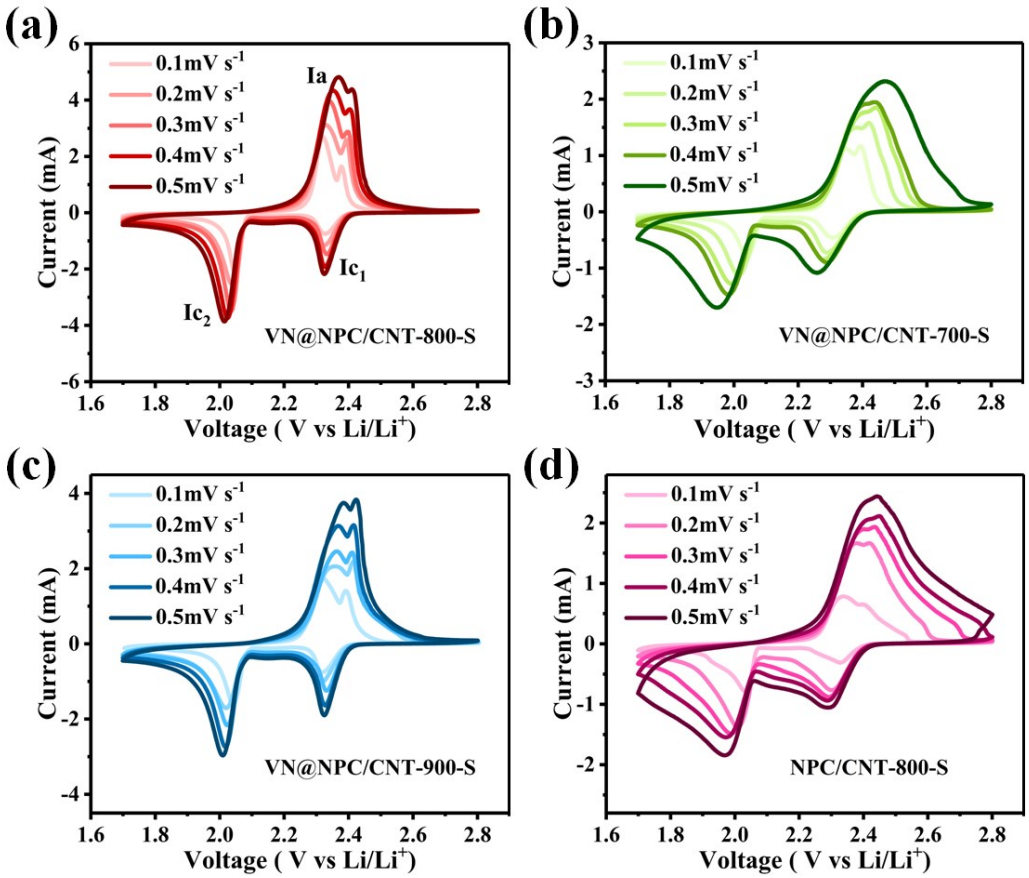


**Fig. S16** CV curves of (a) VN@NPC/CNT-800-S, (b) VN@NPC/CNT-700-S, (c) VN@NPC/CNT-900-S and (d) NPC/CNT-800-S at different sweep rates.

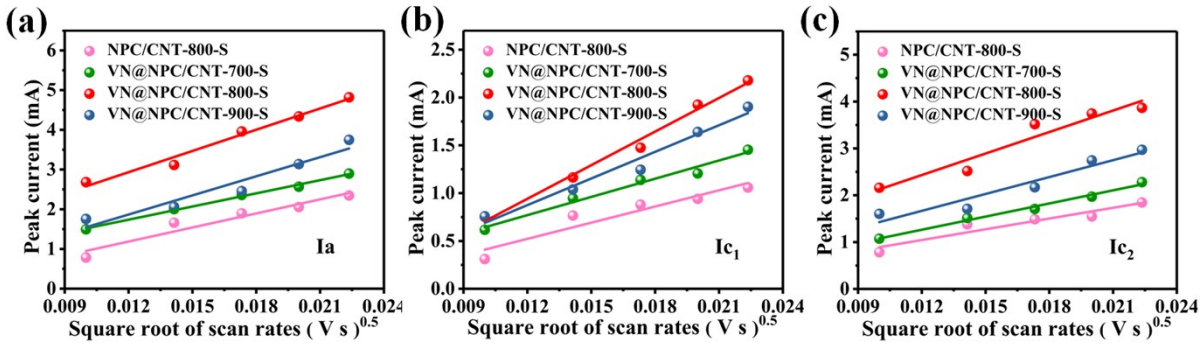


**Fig. S17** CV peak current of VN@NPC/CNT-T and NPC/CNT-800 at different scan rates for (a) the anodic oxidation process (Ia: $Li_2S_2/Li_2S \rightarrow S_8$), (b) the cathodic reduction process 1 ($Ic_1$: $S_8 \rightarrow Li_2S_x$, $4 \leq x \leq 8$), (c) the cathodic reduction process 2 ($Ic_2$: $Li_2S_x \rightarrow Li_2S_2/Li_2S$) versus the square root of the scan rates.

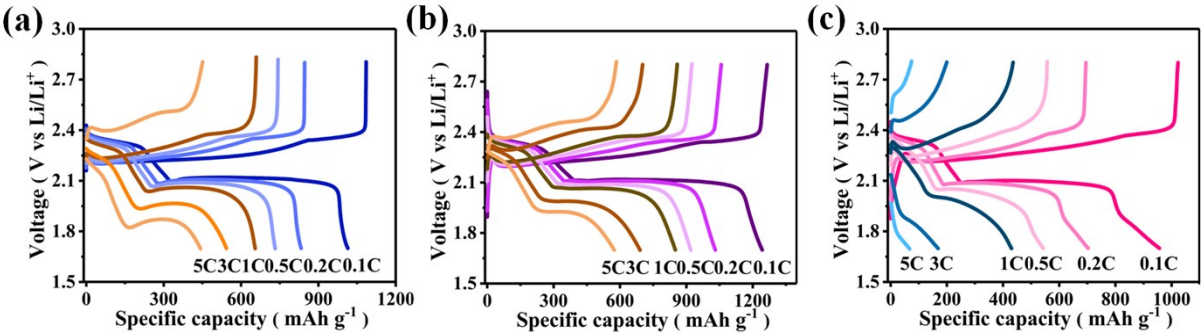


**Fig. S18** Galvanostatic charge-discharge profiles for (a) VN@NPC/CNT-700-S, (b) VN@NPC/CNT-900-S and (c) NPC/CNT-800-S at various rates.

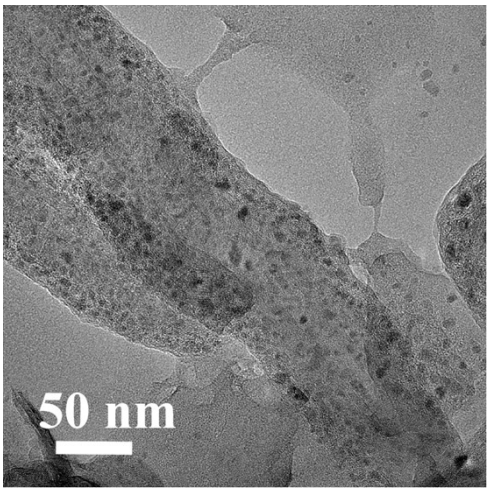


**Fig. S19** TEM image for the cycled VN@NPC/CNT-800-S.

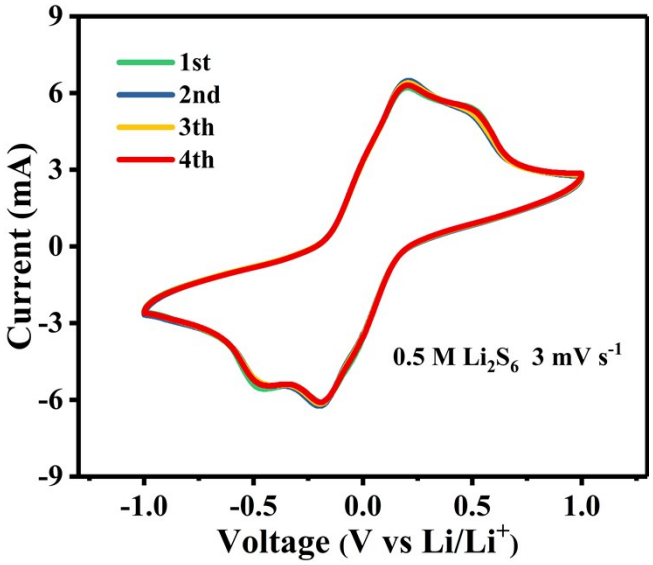


**Fig. S20** Polarization curves of symmetrical cells employing VN@NPC/CNT-800 in 0.5 M $Li_2S_6$ solution at a scan rate of 3 mV $s^{-1}$.

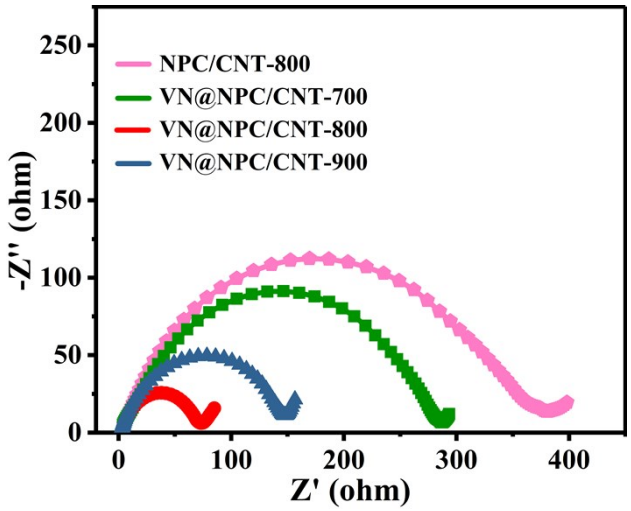


**Fig. S21** EIS spectra of the $Li_2S_6$ symmetrical cell with VN@NPC/CNT-T and NPC/CNT-800 working electrodes in 0.5 M $Li_2S_6$ solution.

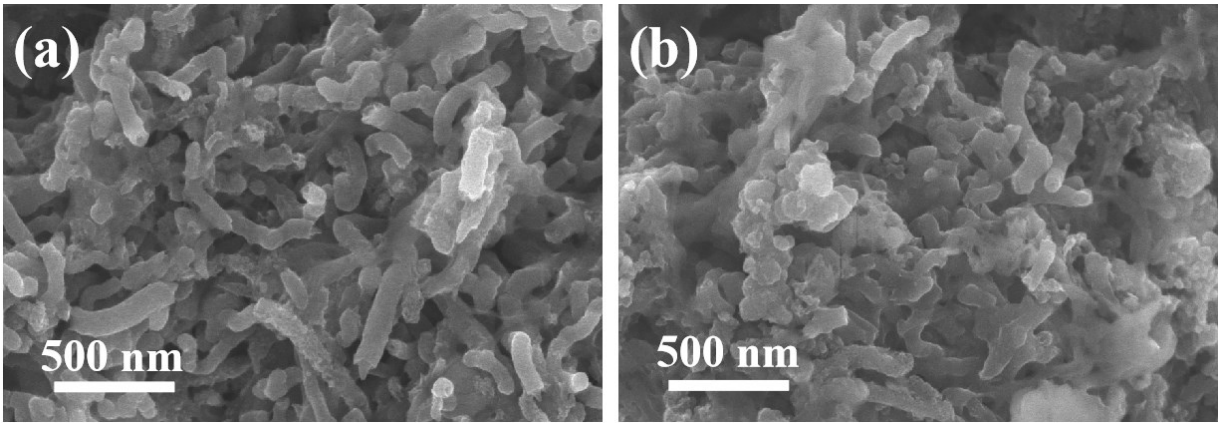


**Fig. S22** SEM images of $Li_2S$ precipitates on the surface of (a) VN@NPC/CNT-800 and (b) NPC/CNT-800.

**Table S1.** Comparison of the electrochemical performance between VN@NPC/CNT-800 and the reported VN-based materials.

| Cathode materials | Sulfur content (wt%) | Sulfur loading (mg $cm^{-2}$) | Current Density | Cycle number | Discharge capacity (mA h $g^{-1}$) | Capacity after cycling (mA h $g^{-1}$) | Capacity decay (%) | Ref. |
|---|---|---|---|---|---|---|---|---|
| **VN@NPC/ CNT-800** | **65** | **2.0** | **5 C** | **1200** | **726** | **417** | **0.035** | **This work** |
| VN/G-S | 60 | 3.0 | 1 C | 200 | 1128 | 917 | 0.09 | [S4] |
| NPC/VN-S | 58 | 0.75 | 1 C | 300 | 734 | 615 | 0.05 | [S5] |
| 78S@VN/N-rGO | 78 | 1.7 | 0.5C | 500 | 1101 | 959 | 0.026 | [S6] |
| S/MVN@CNWs | 57.2 | 2.8 | 1 C | 200 | 1040 | 636 | 0.19 | [S7] |
| S@3$VO_2$–1VN/G | 61.8 | 1.6-1.8 | 2 C | 800 | 1010 | N/A | 0.06 | [S8] |
| S/MoN-VN | 58.5 | 3.0 | 2 C | 500 | 708 | N/A | 0.068 | [S9] |
| VN-NCNFs | N/A | N/A | 1 C | 500 | N/A | 560 | N/A | [S10] |
| Co-VN/S | 69.2 | 1.25 | 3 C | 500 | N/A | 447 | N/A | [S11] |

**References**

[S1] R. Liu, W. Liu, Y. Bu, W. Yang, C. Wang, C. Priest, Z. Liu, Y. Wang, J. Chen, Y. Wang, J. Cheng, X. Lin, X. Feng, G. Wu,Y. Ma and W. Huang, *ACS Nano*, 2020, **14**, 17308-17320.

[S2] X. Yang, S. Chen, W. Gong, X. Meng, J. Ma, J. Zhang, L. Zheng, H. Abruna and J. Geng, *Small*,2020, **16**, 2004950.

[S3] L. Zhu, C. Li, W. Ren, M. Qin and L. Xu, *New J. Chem.*, 2018, **42**, 5109-5116.

[S4] Z. Sun, J. Zhang, L. Yin, G. Hu, R. Fang, H. M. Cheng and F. Li, *Nat. Commun.*, 2017, **8**, 14627.

[S5] W. C. Xu, X. X. Pan, X. Meng, Z. H. Zhang, H. R. Peng, J. Liu and G. C. Li, *Electrochimica Acta*, 2020, **331**, 135287.

[S6] N. Li, Z. Xu, P. Wang, Z. Zhang, B. Hong, J. Li and Y. Lai, *Chem. Eng. J.*, 2020, **398**, 125432.

[S7] X. Li, K. Ding, B. Gao, Q. Li, Y. Li, J. Fu, X. Zhang, P. K. Chu and K. Huo, *Nano Energy,* 2017, **40**, 655-662.

[S8] Z. Song, W. Zhao, L. Kong, L. Zhang, X. Y. Zhu, Y. L. Shao, F. Ding, Q. Zhang, J. Y. Sun and Z. F. Liu, *Energy Environ. Sci.*, 2018, **11**, 2620-2630.

[S9] C. Ye, Y. Jiao, Y H. Y. Jin, A. D. Slattery, K. Davey, H. H. Wang and S. Z. Qiao, *Angew. Chem.*, 2018, **130**, 16945-16949.

[S10] C. Shang, B. Wei, X. Zhang, L. Shui, X. Wang and G. Zhou, *Mater. Lett.*, 2019, **236**, 240-243.

[S11] Z. Z. Cheng, Y. X. Wang, W. J. Zhang and M. Xu, *ACS Applied Energy Mater.*, 2020, **3**, 4523-4530.